Hindawi
International Journal of Photoenergy
Volume 2018, Article ID 8545207, 8 pages
https://doi.org/10.1155/2018/8545207

Research Article

The Reduced Recombination and the Enhanced Lifetime of Excited Electron in QDSSCs Based on Different ZnS and SiO_2 Passivation

Ha Thanh Tung,[1] **Nguyen Thu Thao**,[2] **and Lam Quang Vinh**[3]

[1]*Faculty of Physics, Dong Thap University, Dong Thap Province, Cao Lanh City, Vietnam*
[2]*Ho Chi Minh City University of Science, Ho Chi Minh City, Vietnam*
[3]*Vietnam National University, Ho Chi Minh City, Vietnam*

Correspondence should be addressed to Ha Thanh Tung; httung@dthu.edu.vn

Received 10 January 2018; Revised 24 February 2018; Accepted 6 March 2018; Published 8 April 2018

Academic Editor: Guohua Wu

In this study, we focus on the enhanced absorption and reduced recombination of quantum dot solar cells based on photoanodes which were coated by different ZnS or SiO_2 passivations using the successive ionic layer absorption and reaction methods. The quantum dot solar cells based on photoanode multilayers, which were coated with a ZnS or SiO_2 passivation, increased dramatic absorption in the visible light region as compared with other photoanodes and reduced rapid recombination proccesses in photovoltaic. As a result, the performance efficiency of TiO_2/CdS/CdSe photoanode with SiO_2 passivation increased by 150% and 375% compared with TiO_2/CdS/CdSe with ZnS passivation and TiO_2/CdSe photoanode, respectively. For this reason, we note that the tandem multilayers can absorb more wavelengths in the visible light region to increase a large amount of excited electrons, which are transferred into the TiO_2 conduction band, and decrease number of electrons returned to the polysulfide electrolyte from QDs when a ZnS or SiO_2 passivation is consumed. Moreover, it is obvious that there was a far shift towards long waves in UV-Vis spectra and a sharp drop of intensity in photoluminescence spectra. In addition, the dynamic process in solar cells was carried out by electrochemical impedance spectra.

1. Introduction

In recent years, quantum dot-sensitized solar cells (QDSSCs) based on quantum dots (QDs) have been considerable interest as promising candidates to replace the dye-sensitized solar cells (DSSCs) because QDs have potential functions such as a high extinction coefficient, tunable bandgaps, a large intrinsic dipole moment, low processing cost compared to organic dyes [1, 2], and generation of multiple excitons [3]. The QDs were used in QDSSCs as sensitizers which include PbS [4, 5], PbSeS [6], CdS [7], CdSe [8], CdTe [9], and ZnS [10]. The highest efficiency, which was achieved by Jara et al., was approximately 2.51% for $CuInS_2$ [11] because the electrons in the CB of the QDs moved to the electrolyte and recombined or got blocked. Moreover, tandem multilayers can go up the power conversion efficiency in the QDSSCs. Like for instance, Woo et al. [12] and Ravindran et al. [13] studied the QDSSCs based on the TiO_2/CdS/$CuInS_2$ tandem multilayers and the power conversion efficiency was about 1.47%. This photovoltaic performance was higher than those of the CdS and $CuInS_2$ QDs alone. However, the efficiency was still minor because of increased combination processes at the QDs/TiO_2 surface and plenty of electrons moving to the electrolyte.

Overall, this work illustrates the QDSSCs based on different tandem multilayered photoanodes to enhance absorption in the QDSSCs. In addition, ZnS and SiO_2 coating layer was applied to the TiO_2/CdS/CdSe electrode to reduce recombination and electron movement to the electrolyte. Therefore, the efficiency of the QDSSCs can be an upward trend, particularly, compared with TiO_2/CdS and TiO_2/CdSe photoanodes.

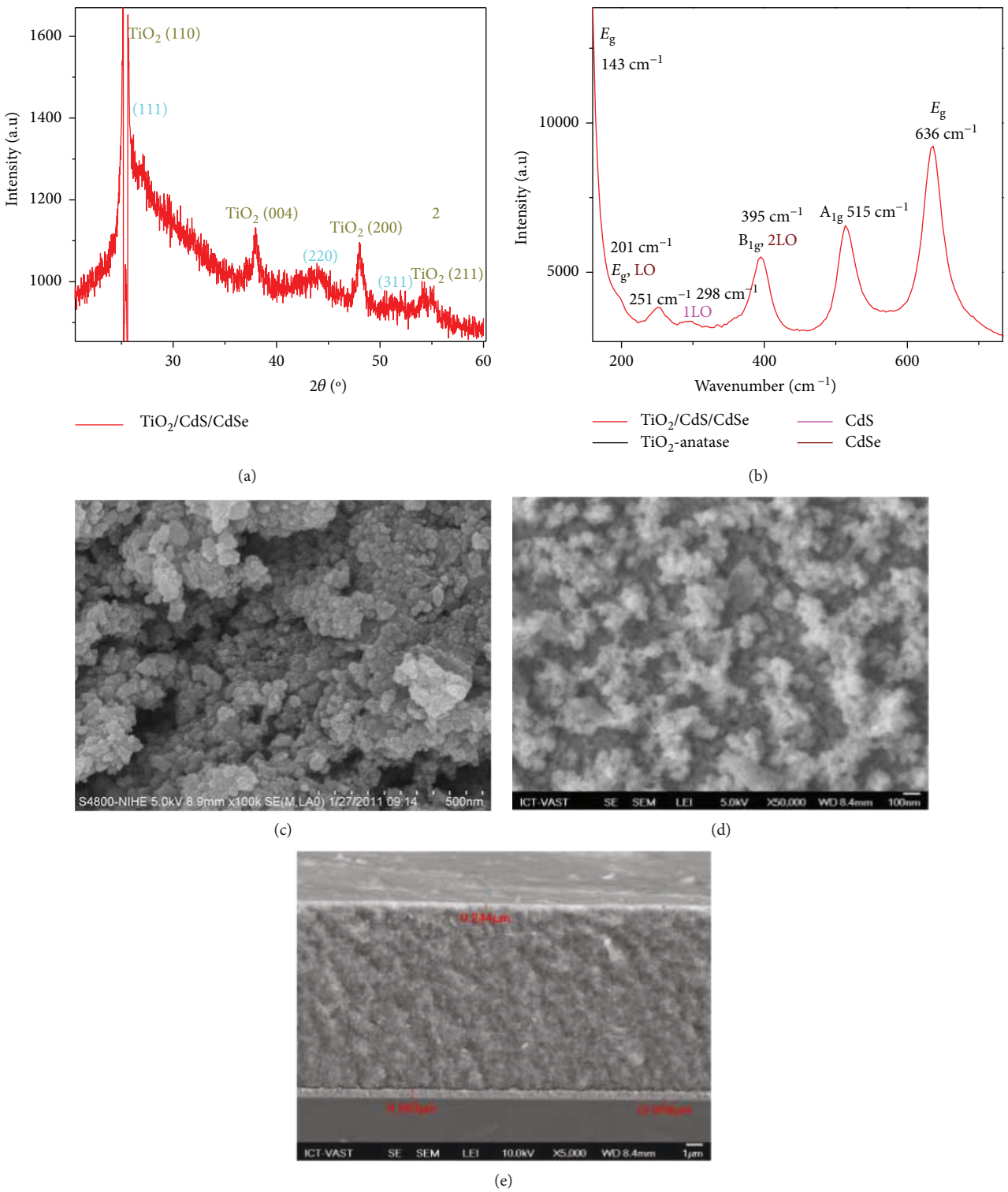

Figure 1: (a) X-ray diffraction patterns, (b) Raman spectra of TiO_2/CdS/CdSe, (c) FESEM images of TiO_2 film, (d) FESEM images of the TiO_2/CdS/CdSe, and (e) cross-sectional FESEM of the TiO_2/CdS/CdSe.

2. Experiment

2.1. Fabrication of TiO_2 Films. There are two types of TiO_2 pastes with different sizes: one type is small nanoparticles of 10–30 nm in which the light can be transmitted to the QDs. Similarly, another is very large particles of 400 nm and it can become the light-scattering centers to orientate to the QDs. The FTO films were coated with TiO_2 layers by silk-screen printing and annealed at 500°C for 30 minutes. Finally, the films were dipped in 40 mmol $TiCl_4$

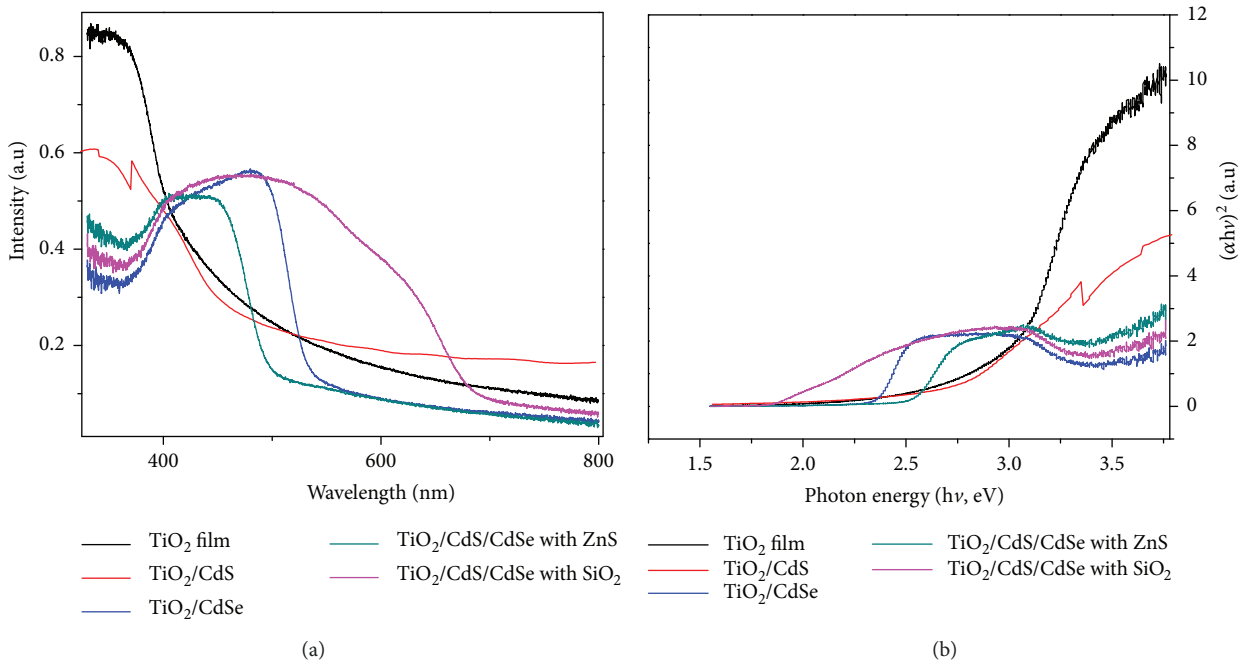

FIGURE 2: (a) UV-Vis of different photoanodes and (b) plot $(\alpha h\nu)^2$ versus the photon energy ($h\nu$) of different photoanodes.

solution for 30 minutes at 70°C and sintered at 500°C for 30 minutes.

2.2. Fabrication of CdS and CdSe-Sensitized Photoanodes with ZnS or SiO_2. A TiO_2/CdS was prepared by the SILAR. Firstly, the TiO_2 film was dipped in 0.5 M Cd^{2+} solution for 1 min and 0.5 M S^{2-} solution for 1 min after being dried in the air to make one SILAR layer. Thickness of the electrode layer showed up in repeat of the three time layers. Secondly, the TiO_2/CdS film was then dipped in Cd^{2+} solution for 5 min and Se^{2-} for 5 min after rinsing with Milli-Q ultrapure water to make one SILAR layer. Thickness of the TiO_2/CdS/CdSe was increased in repeat of the three time layers. Finally, a TiO_2/CdS/CdSe film was dipped in 0.1 M Zn^{2+} solution for 5 min and 0.1 M S^{2-} solution for 5 min after rinsing with Milli-Q ultrapure water to make one SILAR layer. Thickness of the TiO_2/CdS/CdSe with ZnS layer had a growth in repeat the two time layers. Similarly, a TiO_2/CdS/CdSe was immersed in a beaker with an aqueous solution-mixed tetraethyl orthosilicate (0.01 M) and NaOH (0.1 M) during 15 min. After that, the films were rinsed with water and dried in air.

The QDSSCs were prepared with an active area of 0.192 cm^2, a photoanode, and a cathode. The space between photoanode and counter electrode was filled with the polysulfide electrolyte, which consisted of 0.5 M Na_2S, 0.2 M S, and 0.2 M KCl in Milli-Q ultrapure water/methanol (7 : 3 by volume).

2.3. Characterization. The morphologies of samples were investigated using field emission scanning electron microscopy (FESEM). The crystal structure was analyzed using an X-ray diffractometer (Philips, PANalytical X'Pert, CuKα radiation). The absorption properties of the samples were investigated using a diffuse reflectance UV-Vis spectrometer (JASCO V-670). The current-voltage (J-V) characteristics of the QDSSC were measured under AM 1.5 (100 mW/cm^2) illumination, which was provided by a solar simulator (Oriel, USA), and recorded by a Keithley model 2400 digital source meter. Electrochemical impedance spectroscopy (EIS) measurements were obtained by an FRA-equipped PGSTAT-30 from Autolab. The measurements were performed in dark conditions at negative bias, and the frequency range was from 500 kHz to 0.1 Hz with a modulation amplitude of 20 mV.

3. Results and Discussions

3.1. Structure and Morphology of Material. To obtain information about the QDs' size and crystalline photoanodes, the electrodes were annealed in vacuum at 200°C. They were measured by using an X-ray diffractometer (XRD). Figure 1(a) illustrates the XRD of the TiO_2/CdS/CdSe photoanode. As can be seen from Figure 1(a), it is obvious that the XRD of photoanode clearly appears the strongest peak at 25.4° position corresponding to the (101) plane which indicates an upstanding TiO_2 anatase [14]. In addition, the XRD illustrates three peaks at 26.4°, 44°, and 51.6° corresponding to the (111), (220), and (311) planes of CdS and CdSe cubic phase [10]. Similarly, the crystallization of electrode was also determined by Raman spectra. It is noticeable that four modes are observed at 144 cm^{-1}, 397 cm^{-1}, 517 cm^{-1}, and 638.5 cm^{-1} corresponding to phonon vibrations of TiO_2 anatase [15]. Moreover, three peaks also appeared at 206.5 cm^{-1} and 395 cm^{-1}, corresponding to phonons of longitudinal optical vibrations in CdSe and at 298 cm^{-1} corresponding to the longitudinal optical mode in CdS.

To observe shape of the photoanode, FESEM of the TiO_2/CdS/CdSe electrode was carried out. It is obvious that the white TiO_2 electrode became yellow and red because of the

Table 1: The parameters obtained from UV-Vis.

Sample	Wavelength of absorption edge (nm)	E_g (eV)	E_{CB} (eV)	E_{VB} (eV)
TiO_2	443	2.80	−4.3	−7.5
TiO_2/CdS	490	2.53	−4.11	−6.64
TiO_2/CdSe	575	2.16	−4.3	−6.4
TiO_2/CdS/CdSe/ZnS	594	2.09	—	—
TiO_2/CdS/CdSe/SiO_2	679	1.83	—	—

growth of CdS and CdSe (Figure 1(d)), compared to the FESEM of the pure TiO_2 film. Looking at Figure 1(e), this is a cross-sectional FESEM of TiO_2/CdS/CdSe, which is homogeneous and strongly adherent to the substrate and shows cutting shape of film with thickness of 12 μm. This also proves that CdS, CdSe, and QDs have successfully coated on the surfaces of TiO_2.

3.2. The Optical Photoanodes. The optical CdS/CdSe-cosensitized TiO_2 films can be monitored by studying the absorbance and energy bandgap of the materials. Figure 2(a) shows the UV-Vis spectra with distrinct photoanodes. The absorption of the TiO_2/CdS/CdSe with ZnS or SiO_2 passivation electrode is expanded through the visible region compared with other photoanodes. The absorbance of the TiO_2/CdS/CdSe with SiO_2 passivation electrode progresses because the loaded CdS and CdSe concentrations on the TiO_2 film can absorb more photons in the visible region from 400 nm to 700 nm.

We can determine optical bandgap of materials based on the relation between the absorption coefficient (α) and the incident photon energy (hν) using Tauc [16].

$$(a\mathrm{h}\nu) = a_o\left(\mathrm{h}\nu - E_g\right). \quad (1)$$

Besides, to know materials inside, we can also calculate the position of conduction band and valence band for materials, which depend on energy bandgap of materials as follows:

$$E^o_{CB} = E_e - X + 0.5E_g, \quad (2)$$

where

$$X = \left[\left(x^x_{Cd}\right) \times \left(x^y_S\right)\right]^{1/(x+y)} \quad (3)$$

for CdS or

$$X = \left[\left(x^x_{Cd}\right) \times \left(x^y_{Se}\right)\right]^{1/(x+y)} \quad (4)$$

for CdSe, and

$$x_M = 0.5\left[E^M_{EA} + E^M_{ion}\right], \quad (5)$$

with M = Cd, S, and Se. Where E^o_{CB} is the conduction band potential, E_e is a given constant equal 4.5 eV [17]. E_{EA} for Cd, S, and Se are 0 eV, 2.077 eV, and 2.02 eV, respectively. Similarly, E_{ion} for Cd, S, and Se are 8.99 eV, 10.36 eV, and 9.75 eV, respectively. The position of conduction and valence bands of CdS and CdSe are recorded in Table 1. Figure 2(b)

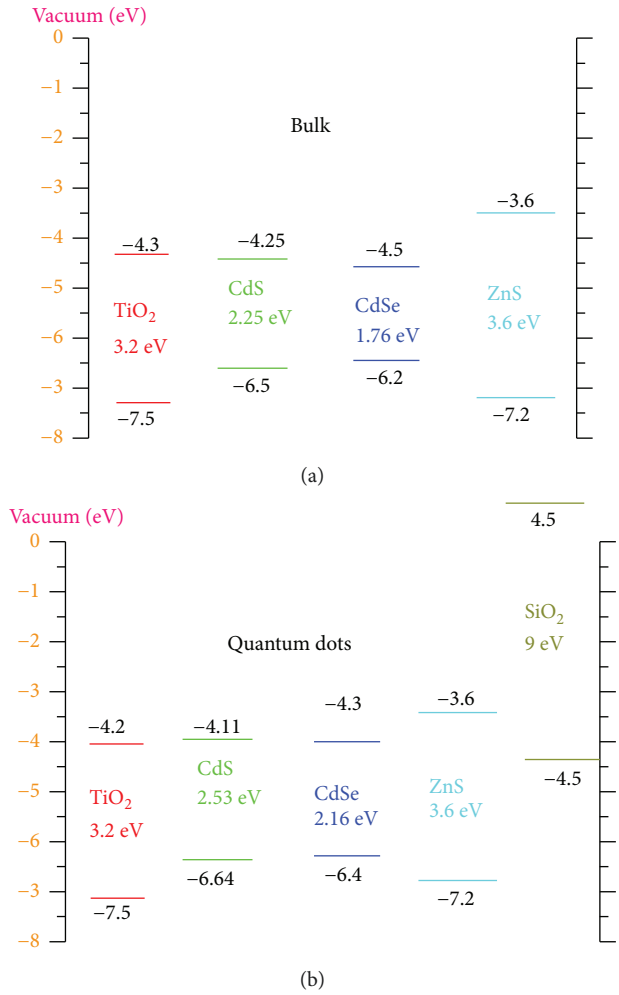

Figure 3: Energy levels alignment of the photoanode: (a) bulk and (b) quantum dots.

can plot $(\alpha\mathrm{h}\nu)^2$ versus the photon energy (hν) using data from the optical absorption spectra. The plotting results are recorded in Table 1. It is immediately remarkable that there is a steadily dropping tendency of energy bandgap from 2.8 eV of pure TiO_2 film to 1.83 eV of TiO_2/CdS/CdSe/SiO_2 film. The obtained results are in good agreement UV-Vis spectra. However, there is a sharp increase in bandgap of CdS and CdSe in bulk and quantum dots. From data in Table 1, it is obvious that the position of conduction and valence bands is shifted toward more negative potential and more positive potential by decreasing the size of particles. Like for instance, the position of conduction and valence bands for CdS shifted toward from −4.25 eV to −4.11 eV and from −6.5 eV to −6.64 eV, respectively. Likewise, the position of conduction and valence bands for CdSe shifted toward between −4.5 eV and− 4.3 eV and between −6.2 eV and− 6.4 eV, respectively (Figures 3(a) and 3(b)). According to the band-edge alignment of CdS and CdSe in Figure 3, the CdS has a high position of conduction band as that of CdSe. Thus, the transfer of excited electrons from CdS to CdSe and TiO_2 facilitates.

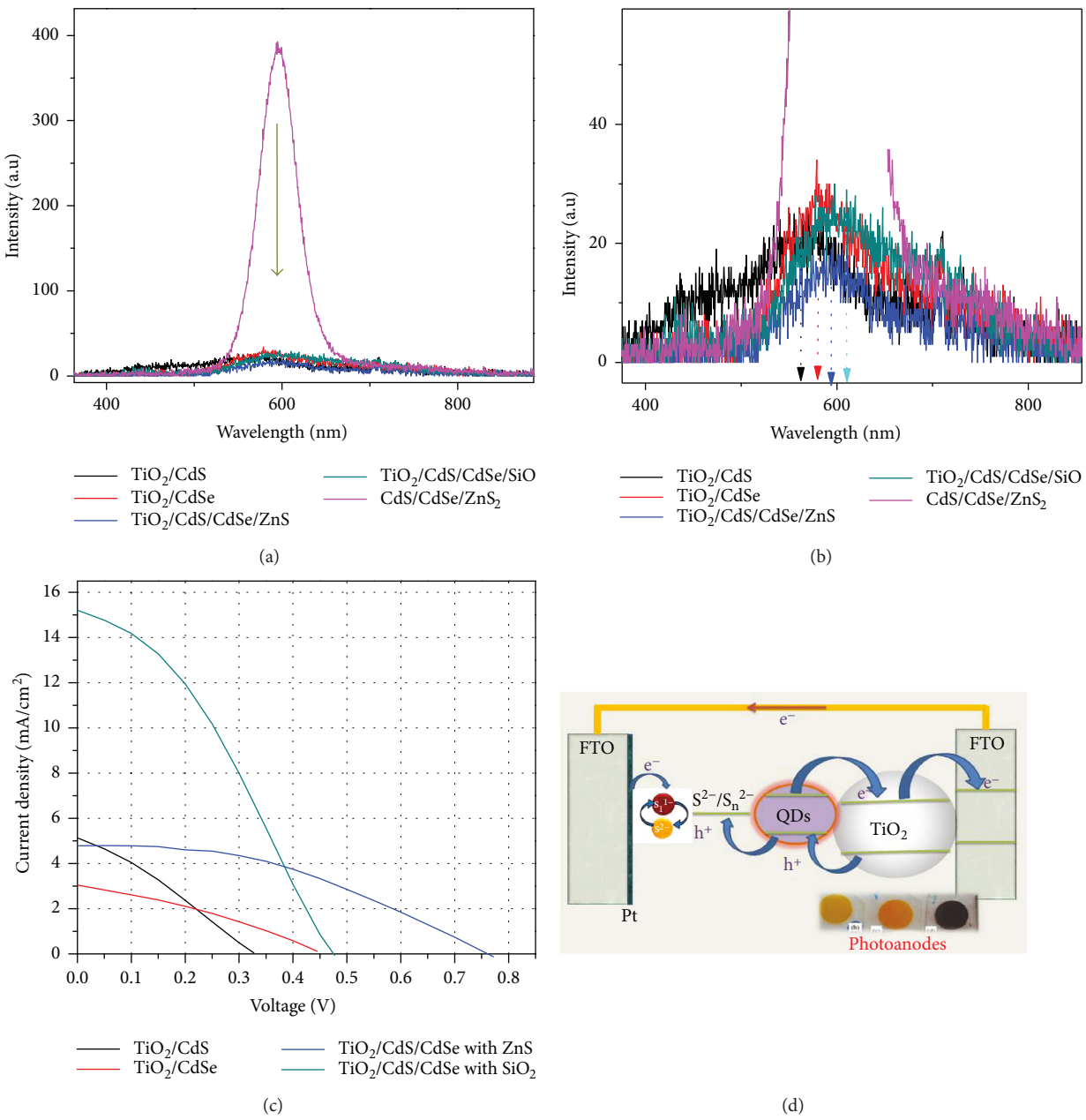

Figure 4: (a, b) Photoluminescence, (c) *J-V* curves of distrinct photoanodes, and (d) structure and energy levels alignment of the QDSSCs.

To study the relative injected electrons in the TiO_2 film from CdS and CdSe QDs, photoluminescence (PL) was carried out (Figures 4(a) and 4(b)). It reveals that there is a significant drop in the PL of TiO_2/CdS, TiO_2/CdSe, TiO_2/CdS/CdSe with ZnS, and TiO_2/CdS/CdSe with SiO_2 photoanodes as compared with that of QD films under identical conditions. The bandgap of TiO_2 (3.2 eV) limits its absorption range below 400 nm. The CdS QDs have a lower CB than CB of CdSe QDs (3 nm size). Therefore, the electron injection from the CB of CdSe QDs to the CB of CdS QDs is effective because CdS and CdSe QDs have a higher quasi Fermi levels than that of TiO_2. Yella et al. reported that when CdS and CdSe QDs were made a cascade structure, the electrons were injected from CdSe to CdS QDs and then to TiO_2 nanoparticles [18]. The redistribution of electrons results in a stepwise band structure. The insertion of a CdS layer between TiO_2 and CdSe elevates the CdSe QDs' CB and generates higher driving force for electron transportation. In addition, the quantum confinement effect makes the energy levels of the CB more negative with decreasing the size of particle [19]. The PL intensity of all photoanodes decreased sharply because the CB of CdSe QDs is as high as that of CdS QDs and TiO_2 nanoparticles. Therefore, the electron injection from the CB of CdSe QDs to the CB of CdS QDs and TiO_2 is effective. Besides, the results reveal that the PL of the anode film loaded with SiO_2 is higher than that of the anode film loaded with ZnS. The possible reason is reduced recombination process in nanoparticles, leading to

Table 2: The value parameters of different QDSSCs obtained from *J-V* curves.

QDSSCs	J_{SC} (mA/cm^2)	V_{OC} (V)	Fill factor (FF)	Efficiency η (%)
TiO_2/CdS	5.5	0.35	0.30	0.7
TiO_2/CdSe	5.87	0.37	0.33	0.88
TiO_2/CdS/CdSe with ZnS	6.01	0.76	0.43	1.92
TiO_2/CdS/CdSe with SiO_2	12.0	0.54	0.46	3.01

increase the PL of nanoparticles. The increase of PL can also boost the emission quantum yield (QY) of QDs, which is helpful for producing more excitons.

3.3. Photovoltaic Performance of the QDSSCs. The characterization by *J-V* curves provides limited resources to analyze the mechanisms that govern the performance. A thorough analysis requires discriminating several factors such as series resistance, recombination parameters, and carrier energetics. These factors are not commonly available simply by analyzing *J-V* curve data, notably because *J-V* curves are elastic with respect the models and can be equally described by many different frameworks. Figure 4(c) illustrates the *J-V* curves of the QDSSCs with distinct photoanodes with sensitized TiO_2 nanoparticles (active area: 0.192 cm^2) at AM 1.5 (100 mW/cm^2). All QDSSCs has appeared the *J-V* characteristic. The performance parameters of QDSSCs are listed in Table 2. The thickness of the QDs was optimized with CdS (3 layers), CdSe (3 layers), and SiO_2 (2 layers) in this work. The TiO_2/CdS/CdSe/SiO_2 exhibits the highest performance: $\eta = 3.01\%$ (we used Pt counter electrode), $V_{OC} = 0.54$ V, $J_{SC} = 12$ mA/cm^2, and FF = 0.46. It is immediately noticeable that J_{SC} of the QDSSCs improved significant after SiO_2 coating and is attributed to the excited electrons characteristics, such as separation, collection, injection, and recombination. The TiO_2/CdS/CdSe was coated with SiO_2 or ZnS passivation which increased the significant light harvesting, separation, collection, and injection but reduced recombination.

3.4. EIS of the QDSSCs. The EIS characteristics were found by Mora-Sero et al. [20] to investigate the dynamic processes in the QDSSCs. We can know the information about charge processes through the QDs/TiO_2/FTO contacts and diffusion processes of the electrons in electrolyte and TiO_2 film. Moreover, the lifetime of electrons can be determined as follows [21].

$$\tau_n = R_{ct2} \cdot \mathrm{CPE}_2. \tag{6}$$

Figure 5 illustrates the EIS of the QDSSCs based on the different photoanodes. The Nyquist plots have three semicircles with different frequencies when the concentration of the photoanodes changes. The semicircle at high frequency (95 Hz–1000 kHz) is small because of the resistance against the electron diffusion in FTO/TiO_2 and Pt/electrolyte surfaces (denoted by R_{ct1}). The semicircle at the intermediate

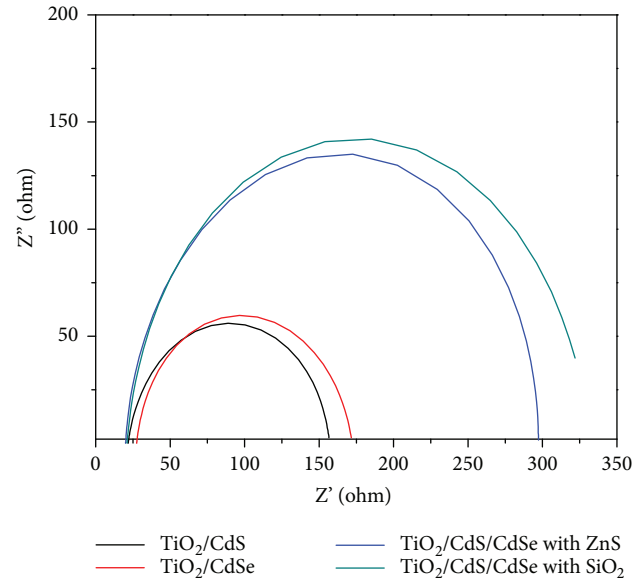

Figure 5: Nyquist of the QDSSCs.

frequency (0.44–95 Hz) is large because of the resistance against the electron diffusion in the TiO_2 film and TiO_2/QDs/electrolyte contacts (denoted by R_{ct2}). The semicircle at low frequency (0.049–0.44 Hz) is because of the diffusion in the S_n^{2-}/S^{2-} electrolyte. R_S is the resistance at the Ag/FTO front and back contacts of the QDSSCs.

Moreover, we also focused on the dynamic resistance in the QDSSCs, which is determined from the *J-V* curves. The external resistance is

$$R_D = \frac{V_1 - V_2}{I_2 - I_1}, \tag{7}$$

the internal resistance is

$$R_d = \frac{1}{\alpha(I_2 - I_1)} \ln\left[\frac{I_{ph} + I_o - I_1}{I_{ph} + I_o - I_2}\right], \tag{8}$$

and the shunt resistance is

$$R_{SH} = \frac{V_{OC}}{I_{ph} - I_o\left(e^{\alpha V_{OC}} - 1\right)}, \tag{9}$$

where V and I are the voltage and current at the point on the *I-V* curve; V_{OC}, I_{ph}, and I_o are the open voltage, short current, and current density saturation, respectively [22]. All resistances are recorded in Table 3.

As can be seen from Figure 5, it is noticeable that the radius of the semicircles increases in the following order: TiO_2/CdS, TiO_2/CdSe, TiO_2/CdS/CdSe with ZnS, and TiO_2/CdS/CdSe with SiO_2 passivation. The semicircles for the QDSSCs with TiO_2/CdS/CdSe with ZnS and TiO_2/CdS/CdSe with SiO_2 retained their shapes, but the radius of the semicircles expanded more because semicircles 1 and 3 were mixed onto semicircle 2. Therefore, we focus on the change of semicircle 2 at the intermediate frequency. Table 3 illustrates that R_{ct2} increased gradually and then peaked at 132 Ω corresponding to TiO_2/CdS/CdSe with SiO_2 passivation because

Table 3: Parameters obtained from the EIS measurements and *J-V* curves.

QDSSCs	R_D (Ω)	R_d (Ω)	R_S (Ω)	R_{SH} (Ω)	R_{ct1} (Ω)	R_{ct2} (Ω)	τ (ms)
TiO_2/CdS	75.3	57.2	24.56	2177	127	8.07	1.592
TiO_2/CdSe	60.8	33.4	27.4	5396	32.2	112	2.005
TiO_2/CdS/CdSe with ZnS	68.6	53.1	35.5	5472	103	174	2.016
TiO_2/CdS/CdSe with SiO_2	92.5	74.5	53.8	13,000	179	132	2.528

of the increase of thickness photoanode. On the contrary, the result from Table 2 gives that the efficiency of QDSSCs-based TiO_2/CdS/CdSe with SiO_2 photoanode is the highest (3.01%). This means that SiO_2 layer is a passivation to protect CdS and CdSe QDs from electrolyte [23–28] and reduced recombination processes at surface contacts and diffusion in the TiO_2 film. In addition to this, I suppose that there was an increase of the electron lifetime of TiO_2/CdS/CdSe with SiO_2 photoanode-sensitized solar cells and which is near twice that of other photoanode-sensitized solar cells. With this lifetime, the excited electrons are enough time to transfer from CdSe and CdS to TiO_2. Thus, the current density of QDSSCs increased sharply. This result is also consistent with that of UV-Vis spectra, PL spectra, and *J-V* curves. In the same way, the values of resistance dynamic R_s, R_D, and R_d enhanced minor while the thickness of photoanodes went up. The results show that the resistance values depended on the thickness of the QD films. External and internal resistances at the same bias voltage under similar illumination conditions are distinct. This is due to the voltage-dependent nature of R_d. The dissimilar nature of R_d at different illuminating conditions is also noted. This can be expected as the values of diode factor at different illuminations are not the same. R_d and R_D of each illumination condition can differ approximately 40%. Therefore, a clear distinction should be made when one studies and measures the two types of dynamic resistance.

4. Conclusions

In summary, we have successfully enhanced performance QDSSCs based on the distinct electrodes with ZnS or SiO_2 passivation. The highest efficiency of the QDSSCs based on the TiO_2/CdS/CdSe with SiO_2 passivation electrode is approximately 3.01%, and the short current density is 12 mA/cm^2 compared with that of other electrodes because ZnS or SiO_2 passivation protected CdS and CdSe QDs from electrolyte and reduced recombination processes at surface contacts and diffusion in the TiO_2 film.

Data Availability

The data used to support the findings of this study are available from the corresponding author upon request.

Conflicts of Interest

The authors declare no competing interests.

Acknowledgments

This research is funded by the Vietnam National Foundation for Science and Technology Development (NAFOSTED) under Grant no. 103.03-2016.94. The authors would like to thank Ho Chi Minh City University of Science, Vietnam.

References

[1] P. V. Kamat, "Quantum dot solar cells. Semiconductor nanocrystals as light harvestors," *The Journal of Physical Chemistry C*, vol. 112, no. 48, pp. 18737–18753, 2008.

[2] A. Nozik, "Quantum dot solar cells," *Physica E: Low-dimensional Systems and Nanostructures*, vol. 14, no. 1-2, pp. 115–120, 2002.

[3] M. C. Beard, "Multiple exciton generation in semiconductor quantum dots," *The Journal of Physical Chemistry Letters*, vol. 2, no. 11, pp. 1282–1288, 2011.

[4] S. S. Mali, S. K. Desai, S. S. Kalagi et al., "PbS quantum dot sensitized anatase TiO_2 nanocorals for quantum dot-sensitized solar cell applications," *Dalton Transactions*, vol. 41, no. 20, pp. 6130–6136, 2012.

[5] J. Jie, Z. Zheng-Ji, Z. Wen-Hui, and W. Si-Xin, "CdS and PbS quantum dots co-sensitized TiO_2 nanorod arrays with improved performance for solar cells application," *Materials Science in Semiconductor Processing*, vol. 16, no. 2, pp. 435–440, 2013.

[6] N. P. Benehkohal, V. González-Pedro, P. P. Boix et al., "Colloidal PbS and PbSeS quantum dot sensitized solar cells prepared by electrophoretic deposition," *The Journal of Physical Chemistry C*, vol. 116, no. 31, pp. 16391–16397, 2012.

[7] Q. Zhang, Y. Zhang, S. Huang et al., "Application of carbon counterelectrode on CdS quantum dot-sensitized solar cells (QDSSCs)," *Electrochemistry Communications*, vol. 12, no. 2, pp. 327–330, 2010.

[8] G.- P. Victoria, X. Xueqing, M.-S. Ivan, and B. Juan, "Modeling high-efficiency quantum dot sensitized solar cells," *ACS Nano*, vol. 4, no. 10, pp. 5783–5790, 2010.

[9] Y. Zusing and C. Huan-Tsung, "CdHgTe and CdTe quantum dot solar cells displaying an energy conversion efficiency exceeding 2%," *Solar Energy Materials and Solar Cells*, vol. 94, no. 12, pp. 2046–2051, 2010.

[10] N. Balis, V. Dracopoulos, K. Bourikas, and P. Lianos, "Quantum dot sensitized solar cells based on an optimized combination of ZnS, CdS and CdSe with CoS and CuS counter electrodes," *Electrochimica Acta*, vol. 91, pp. 246–252, 2013.

[11] D. H. Jara, S. J. Yoon, K. G. Stamplecoskie, and P. V. Kamat, "Size-dependent photovoltaic performance of $CuInS_2$ quantum dot-sensitized solar cells," *Chemistry of Materials*, vol. 26, no. 24, pp. 7221–7228, 2014.

[12] J. S. Woo, K. Jae-Hong, K. Hyunsoo, C. Chel-Jong, and A. K. Soon, "ZnS overlayer on *in situ* chemical bath deposited CdS quantum dot-assembled TiO_2 films for quantum dot-sensitized solar cells," *Current Applied Physics*, vol. 12, no. 6, pp. 1459–1464, 2012.

[13] T. R. Ravindran, A. K. Arora, B. Balamuruga, and B. R. Mehta, "Inhomogeneous broadening in the photoluminescence spectrum of CdS nanoparticles," *Nano Structured Materials*, vol. 11, no. 5, pp. 603–609, 1999.

[14] R. Vogel, K. Pohl, and H. Weller, "Sensitization of highly porous, polycrystalline TiO_2 electrodes by quantum sized CdS," *Chemical Physics Letters*, vol. 174, no. 3-4, pp. 241–246, 1990.

[15] G. I. Koleilat, L. Levina, H. Shukla et al., "Efficient, stable infrared photovoltaics based on solution-cast colloidal quantum dots," *ACS Nano*, vol. 2, no. 5, pp. 833–840, 2008.

[16] C. Xing, Y. Zhang, W. Yan, and L. Guo, "Band structure-controlled solid solution of Cd_{1-x} Zn_xS photocatalyst for hydrogen production by water splitting," *International Journal of Hydrogen Energy*, vol. 31, no. 14, pp. 2018–2024, 2006.

[17] M. Askari, N. Soltani, E. Saion, W. M. Mat Yunus, M. Erfani, and H. M. Dorostkar, "Structural and optical properties of PVP-capped nanocrystalline $Zn_xCd_{1-x}S$ solid solutions," *Superlattices and Microstructures*, vol. 81, pp. 193–201, 2015.

[18] A. Yella, H.-W. Lee, H. N. Tsao, C. Yi, A. K. Chandiran, and M. K. Nazeeruddin, "Porphyrin-sensitized solar cells with cobalt (II/III)–based redox electrolyte exceed 12 percent efficiency," *Science*, vol. 334, no. 6056, pp. 629–634, 2011.

[19] A. Kongkanand, K. Tvrdy, K. Takechi, M. Kuno, and P. V. Kamat, "Quantum dot solar cells. Tuning photoresponse through size and shape control of CdSe–TiO_2 architecture," *Journal American Chemistry Society*, vol. 130, no. 12, pp. 4007–4015, 2008.

[20] I. Mora-Sero, S. Gimenez, T. Moehl et al., "Factors determining the photovoltaic performance of a CdSe quantum dot sensitized solar cell: the role of the linker molecule and of the counter electrode," *Nanotechnology*, vol. 19, no. 42, article 424007, 2008.

[21] Q. Wang, S. Ito, M. Gratzel et al., *The Journal of Physical Chemistry B*, vol. 110, no. 50, pp. 25210–25221, 2006.

[22] J. Thongpron, K. Kirtikara, and C. Jivacate, "A method for the determination of dynamic resistance of photovoltaic modules under illumination," in *Proceeding of Technical Digest of the 14th International Photovoltaic Science and Engineering Conference—PVSEC14*, Bangkok, Thailand, January 2004https://vi.scribd.com/document/213502631/Thongpron-Kirtikara-Jivacate-2006-a-Method-for-the-Determination-of-Dynamic-Resistance-of-Photovoltaic-Modules-Under-Illumination.

[23] A. Ju-Hyun, R. S. Mane, V. V. Todkar, and S.-H. Han, "Invasion of CdSe nanoparticles for photosensitization of porous TiO_2," *International Journal of Electrochemistry Science*, vol. 2, pp. 517–522, 2007.

[24] T. H. Thanh, V. L. Quang, and H. T. Dat, "Influence of surface treatment and annealing temperature on the recombination processes of the quantum dots solar cells," *Journal of Nanomaterials*, vol. 2016, Article ID 9806386, 9 pages, 2016.

[25] T. T. Ha, C. H. Chi, N. Vy, N. T. Thoa, T. D. Huynh, and Q. V. Lam, "Improving the performance of QDSSCs based on Tio_2/CdS (Silar)/CdSe(Colloid)/Zns(Silar) photoanodes," *Environmental Progress & Sustainable Energy*, vol. 34, no. 6, pp. 1774–1779, 2015.

[26] T. H. Thanh, V. L. Quang, and D. H. Thanh, "Determination of the dynamic resistance of the quantum dots solar cells by one I–V curve and electrochemical impedance spectra," *Solar Energy Materials and Solar Cells*, vol. 143, pp. 269–274, 2015.

[27] T. H. Thanh, L. Q. Vinh, and H. T. Dat, "The dynamic resistance of CdS/CdSe/ZnS co-sensitized TiO_2 solar cells," *Brazilian Journal of Physics*, vol. 44, no. 6, pp. 746–752, 2014.

[28] J. Chang, T. Oshima, S. Hachiya et al., "Uncovering the charge transfer and recombination mechanism in ZnS-coated PbS quantum dot sensitized solar cells," *Solar Energy*, vol. 122, pp. 307–313, 2015.